Atmos. Chem. Phys. Discuss.,
https://doi.org/10.5194/acp-2018-1312-AC2, 2020

Atmospheric Chemistry and Physics Discussions

Interactive comment on "Tropical Pacific Climate Variability under Solar Geoengineering: Impacts on ENSO Extremes" *by* Abdul Malik et al.

Abdul Malik et al.

abdul.malik@kaust.edu.sa

Received and published: 29 August 2020

The authors thank to both referees for their comments and suggestions, which have greatly helped us to improve our manuscript. Below, we reply point-by-point, highlighting the changes we have implemented. The primary concern of the referees was the evaluation of the climate model capability to simulate ENSO variability, and the lack of detailed explanations on possible mechanisms responsible for changes in ENSO both under 4$\times$CO2 and solar geoengineering (G1). In the revised manuscript, we therefore put a strong emphasis on model evaluation and are able to confirm the necessary model skill (section 2.4). We also provide an entirely new section (section 4) on possible mechanisms behind the changes in ENSO extremes and ENSO amplitudes.

Major Points

1)

To study the ENSO changes under solar geoengineering, the results are all based on one single model HadCM3L. In Cai et al. (2014) and Collins et al. (2001), the model they used is HadCM3. I admit that HadCM3L and HadCM3 are identical in most aspects, but there are still differences between these two simulations. The differences should be mentioned in this study because the HadCM3L may not be skillful in reproducing ENSO variabilities, and thus the sentence in P4 L32-33 may not be completely correct. I suggest that the ENSO simulated in HadCM3L should be addressed first, regarding its magnitude and pattern. For instance, the EOF analyses can be carried out on the piControl simulations. It will help us to have a general idea of how capable the HadCM3L is in simulating the ENSO and its diversity, and what's the biases compared with observations. As pointed out in Cai et al. (2018), the magnitude and location of ENSO events are inconsistent among models. The averaged SSTA in a fixed box to measure the intensity of ENSO can be tricky. A look at the ENSO pattern in HadCM3L can also facilitate a better ENSO extreme definition, i.e. the Nino indices may not be best to define ENSO intensity. At least, a glimpse of the Figure 8 reveals that ENSO simulation is not good enough, especially the shape, maximum location and horseshoe-shaped cold SSTA in the western Pacific during El Nino events.

Reply:

We have deleted the text referring to P4 and L32-33 in the revised manuscript. In the revised manuscript we have evaluated the model skill for reproducing ENSO diversity following Cai et al. (2018). The HadCM3L belongs to the family of HadCM3 models; the only difference between HadCM3 and HadCM3L is lower ocean resolution. We have included a separate section on model evaluation. We have also mentioned the apparent biases in HadCM3L compared to observations. We find that HadCM3L has a reasonable skill to simulate ENSO and can be employed for the current study. The

HadCM3L simulates the sea surface temperature maximum anomaly pattern over the Niño3 region. In the revised manuscript, we have made the following additions:

HadCM3L stems from the family of HadCM3 climate models; the only difference is lower ocean resolution (HadCM3: 1.25o $\times$ 1.25o; Valdes et al., 2017). (see section 2.1, page 4, lines 25-27)

Before employing HadCM3L for studying ENSO variability under 4$\times$CO2, and G1, we evaluate its piControl simulation against present-day observational data. (see section 2.4, page 6, lines 40-41)

Further, we have included the following paragraphs (section 2.4, page 7, and line 14 to next page line 21):

In addition, we evaluate the ENSO modelled by HadCM3L following a principal component (PC) approach suggested by Cai et al. (2018). Considering distinct eastern and central Pacific ENSO regimes based on Empirical Orthogonal Function (EOF) analysis, they found that climate models capable of reproducing present-day ENSO diversity show a robust increase in eastern Pacific ENSO amplitude in a greenhouse warming scenario. Specifically, the approach assumes that any ENSO event can be represented by performing EOF analysis on monthly SST anomalies and combining the first two principal patterns (Cai et al., 2018). The first two PCs time series, PC1 and PC2, show a non-linear relationship in observational datasets (Fig. S1m). Climate models that do not show such a non-linear relationship cannot satisfactorily reproduce ENSO diversity, and hence are not sufficiently skilful for studying ENSO properties (Cai et al., 2018). Here, we perform EOF analysis on quadratically detrended monthly SST and wind stress anomalies of ERA5 and piControl over a consistent period of 41-year. We evaluate HadCM3L's ability to simulate two distinct ENSO regimes and the non-linear relationship between the first two PCs, i.e., PC2(t) = α[PC1(t)]^2 + β[PC1(t)]^2 + γ (Fig. S1). From ERA5, α = -0.36 (statistically significant at 99 % confidence level, hereafter "cl") whereas in piControl α = -0.31 (99 % cl), which is same as the mean α = -0.31

value calculated by Cai et al. (2018) averaged over five reanalysis datasets. The 1st and 2nd EOF patterns of monthly SST and wind stress anomalies of piControl (Fig. S1 b, e) are comparable with that of ERA5 (Fig. S1 a, d). EOF1 of piControl shows slightly stronger warm anomalies in the eastern equatorial Pacific, whereas negative anomalies over the western Pacific are slightly weaker compared to ERA5. In EOF1, the stronger wind stress anomalies occur to the west of the Niño3 region, which is a characteristic feature during the eastern Pacific El Niño events (see Kim and Jin 2011a). Compared to ERA5, the spatial pattern of warm eastern Pacific anomalies is slightly stretched westwards, and wind stress anomalies are relatively stronger over the equator and South Pacific Convergence Zone (SPCZ). The 2nd EOF, in both ERA5 and piControl, shows warm SST anomalies over the equatorial central Pacific Niño4 region. The variance distributions for ERA5 and HadCM3L match well for EOF1 (ERA5: 82 %, piContol: 90 %) whereas a large difference exist for EOF2 (ERA5: 18 %, piControl: 10 %).

The PCA is also useful for evaluating how well HadCM3L represents certain types of ENSO events. Eastern and central Pacific ENSO events can be described by an E-Index (PC1-PC2)/$\sqrt{2}$), which emphasizes maximum warm anomalies in the eastern Pacific region, and a C-Index (PC1+PC2)/$\sqrt{2}$) respectively, which focuses on maximum warm anomalies in the central Pacific (Cai et al., 2018). Here, we show the eastern Pacific (EP) Pattern (Fig. S1 g, h) and central Pacific (CP) pattern (Fig. S1 j, k) by linear regression of mean DJF E- and C-Index, respectively, onto mean DJF SST and wind stress anomalies. We find that model's EP and CP patterns agree reasonably well with that of ERA5. HadCM3L underestimates the E-index skewness (1.16) whereas overestimates the C-Index skewness (-0.89) compared to ERA5 (2.08 and -0.58 respectively) averaged over DJF. HadCM3L's performance averaged over the entire simulated period of piControl is also consistent with ERA5 (Fig. S1; α: -0.32, EOF1: 64 %, EOF2, 8%, E-index skewness: 1.30, C-index skewness: -0.42). In general, in HadCM3L, the contrast between the E- and C-index skewness over the entire simulated period is sufficient enough to differentiate relatively strong warm (cold) events in the eastern (central)

equatorial Pacific compared to the central (eastern) equatorial Pacific. Finally, we also evaluated the hf and BJ feedbacks which, for piControl, are very similar to those of ERA5 (Table S5-6).

We conclude that HadCM3L has a reasonable skill for studying long-term ENSO variability and its response to solar geoengineering. However, we also highlight the need for and hope to motivate future modelling studies that will help identify model dependencies in the ENSO response.

Please see Supplementary Fig. S1 and Tables S5-S6 as well.

2)

The change of extreme ENSO under solar geoengineering is a major concern in this study. This paper shows adequate results to uncovering the phenomenon that may happen but lacks the investigations on underlying mechanisms. The magnitude of ENSO is mainly driven by the positive and negative feedbacks involving air-sea interactions. In the manuscript, the major atmospheric and oceanic components are depicted, such as the thermocline, zonal wind stress and zonal SST gradient. A clear physical process is needed to understand how ENSO can be modified in G1 and 4_CO2. The Bjerknes feedback, thermocline feedback and heat flux feedback can be evaluated under different scenarios. This may be helpful to illustrate why ENSO in G1 can be modified even though the thermocline, zonal SST gradient and zonal wind stress are not well separated in G1 and piControl. Also, it's necessary to go deeper into the reason why the responses of El Nino and La Nina are different for magnitude change and same for frequency change.

Reply:

In the revised manuscript, we have calculated ENSO feedbacks, Bjerknes and heat flux, and ocean stratification to explain the mechanisms for change in ENSO. We have added Section 4 elaborating on the mechanism for change in ENSO under both 4xCO2

and G1. (See section 4, from page 17 and line 1 to page 18 and line 29). Specifically we write:

4 Mechanisms behind the changes in ENSO variability

4.1 Under greenhouse gas forcing

The reduced ENSO amplitude under 4$\times$CO2 is mainly caused by stronger hf and weaker BJ feedback relative to piControl (Fig. 15a-b, and Table S5-6). More rapid warming over the eastern than western equatorial Pacific regions reduces the SST asymmetry between western and eastern Pacific (Fig. 1d), resulting in the weakening of ZSSTG (Fig. 4b) that significantly weakens the zonal winds stress (Fig. 4a) and hence PWC (Fig. 6b, d, see Bayr et al., 2014). The overall reduction of zonal wind stress reduces the BJ feedback, which, in turn, can weaken the ENSO amplitude. Climate models show an inverse relationship between hf feedback and ENSO amplitude (Lloyd et al., 2009, 2011; Kim and Jin 2011b). The increased hf feedback might be the result of enhanced clouds due to strengthened convection (Fig. 5b, d) and stronger evaporative cooling in response to enhanced SSTs under 4$\times$CO2 (Knutson and Manabe 1994; Kim and Jin 2011b). Kim and Jin (2011a, b) found intermodel consensus on the strengthening of hf feedback in CMIP3 models under enhanced GHG warming scenario (Ferret and Collins 2019). Further, we see increased ocean stratification under 4$\times$CO2 (Fig. 15d and Table S7). A more stratified ocean is associated with an increase in both the El Niño events and amplitude in the eastern Pacific (Wang et al. 2020). It can also modify the balance between feedback processes (Dewitte et al., 2013). Enhanced stratification may also cause negative temperature anomalies in the central to the western Pacific through changes in thermocline tilt (Dewitte et al., 2013). Since the overall ENSO amplitude decreases in our 4xCO2 simulation, we, thus, conclude that the ocean stratification mechanisms cannot be the dominant factor here, but that hf and BJ feedbacks must more than cancel out the effect of ocean stratification on ENSO amplitude.

The increased frequency of extreme El Niño events under 4×CO2 is due to change in the mean position of the ITCZ (Fig. S2), causing frequent reversals of MSSTG (Fig. S3), and eastward extension of the western branch of PWC (Fig. 6), which both result in increased rainfall over the eastern Pacific (see Wang et al. 2020). This is due to greater east equatorial than off-equatorial Pacific warming (see Cai et al. 2020), which shifts the mean position of ITCZ towards the equator (Fig. S2). Simultaneously more rapid warming of the eastern than western equatorial Pacific reduces the ZSSTG, and hence zonal wind stress, as also evident from the weakening and shift of the PWC (Fig. 6) and increased instances of negative ZSSTG anomalies (Fig. S9). Ultimately, this leads to more frequent vigorous convection over the Niño3 region (Fig. 5d), and enhanced rainfall (Fig. 2d, S8). Therefore, despite the weakening of the ENSO amplitude under 4×CO2, rapid warming of the eastern equatorial Pacific causes frequent reversals of meridional and zonal SST gradients, resulting in an increased frequency of extreme El Niño events (see also Cai et al., 2014; Wang et al., 2020).

We note that under GHG forcing, HadCM3L does not simulate an increase in the frequency of extreme La Niña events as found by Cai et al. (2015b) using CMIP5 models. However, it does show an increase in the total number of La Niña events (Table S4). In a multimodel ensemble mean, Cai et al. (2015b) found that the western Pacific warms more rapidly than the central Pacific under increased GHG forcing, resulting in strengthening of the zonal SST gradient between these two regions. Strengthening of this zonal SST gradient and increased vertical upper ocean stratification provide conducive conditions for increased frequency of extreme La Niña events (Cai et al., 2015b). One reason why we do not see an increase in the frequency of central Pacific extreme La Niña events might be that HadCM3L does not simulate more rapid warming of the western Pacific compared to the central Pacific as noticed by Cai et al. (2015b) (compare our Fig. 1d with Fig. 3b in Cai et al., 2015b), hence, as stronger zonal SST gradient does not develop, across the equatorial Pacific, as needed for extreme La Niña events to occur (see Fig. S9a, c and S10).

4.2 Under solar geoengineering

G1 over cools the upper ocean layers, whereas the GHG-induced warming in the lower ocean layers is not entirely offset, thus increasing ocean stratification (Fig. 15). The increased stratification boosts atmosphere-ocean coupling (see Cai et al., 2018), which favours enhanced westerly wind bursts (Fig. 4a) (e.g., Capotondi et al., 2018) to generate stronger SST anomalies over the eastern Pacific (Wang et al. 2020). The larger cooling of the western Pacific than the eastern Pacific can also enhance westerly wind bursts reinforcing the BJ feedback and hence SST anomalies in the eastern Pacific. We conclude that increased ocean stratification, along with stronger BJ feedback, is the most likely mechanism behind the overall strengthening of ENSO amplitude under G1.

The increased frequency of extreme El Niño events under G1 can be linked to the changes in MSSTG and ZSSTG (see Cai et al., 2014, and Fig. S3, S9). The eastern off-equatorial Pacific cools more than the eastern equatorial regions, providing relatively more conducive conditions for convection to occur through a shift of ITCZ over to the Niño3 region (Fig. 1e). At the same time, the larger cooling of the western equatorial Pacific than of the eastern equatorial Pacific reduces the ZSSTG and convective activity over the western Pacific, which leads to a weakening of the western branch of PWC (Fig. 6e). Hence we see reduced rainfall over the western Pacific and enhanced rainfall from the Niño3 to the central Pacific region (Fig 2e). These mean state changes, strengthening of convection between ∼140o W and ∼150o E, and more reversals of the MSSTG and ZSSTG (Fig. S3) result in an increased number of extreme El Niño events in G1 than in piControl (Fig. 7).

In the Discussion and conclusion (section 5, page 19, lines 1-14), we have added the following paragraph:

To conclude, solar geoengineering can compensate many of the GHG-induced changes in the tropical Pacific, but, importantly, not all of them. In particular, con-

trolling the downward shortwave flux cannot correct one of the climate system's most dominant modes of variability, i.e., ENSO, wholly back to preindustrial conditions. The ENSO feedbacks (Bjerkness and heat flux) and more stratified ocean temperatures may induce ENSO to behave differently under G1 than under piControl and 4×CO2. Different meridional distributions of shortwave and longwave forcings (e.g., Nowack et al., 2016) resulting in the surface ocean overcooling, and residual warming of the deep ocean are the plausible reasons for the solar geoengineered climate not reverting entirely to the preindustrial state. However, we note that this is a single model study, and more studies are needed to show the robustness and model-dependence of any results discussed here, e.g. using long-term multimodel ensembles from GeoMIP6 (Kravitz et al., 2015), once the data are released. The long-term Stratospheric Aerosol Geoengineering Large Ensemble (GLENS; Tilmes et al., 2018) data can also be explored to investigate ENSO variability under geoengineering.

3)

This manuscript pays a lot of efforts on how mean state of tropical Pacific might be modified under 4_CO2 and G1. A connection between mean state change and ENSO change is simply built by using the previously proposed conclusions, i.e. the reduction of MSSTG in both 4_CO2 and G1 indicate increase of extreme El Nino. However, more detailed explanations should be reviewed before applying this theory.

Reply:

In the revised manuscript, we have tested the change in frequency under both 4×CO2 and G1, relative to piControl, first by using rainfall > 5 mm day-1 as a threshold for extreme El Niño events and then selecting only those events for which rainfall > 5 mm day-1 and MSSTG < 0. Both methods show a statistically significant increase in extreme El Niño events. Choosing extreme events having MSSTG < 0 assures that strong convection has established over the Niño3 region during the extreme. Further, we have shown the histograms of MSSTG for all samples and exclusively for extreme

El Niño events, which indicate more frequent reversals of MSSTG both under 4×CO2 and G1 relative to piControl. See also the discussion on mechanism now presented in Sect. 4 and included in a response above. In the revised manuscript, we have further incorporated the following changes:

A threshold of detrended Niño3 total rainfall of 5 mm day-1 recognizes events as extremes even when the MSSTG is positive and stronger, especially under 4×CO2, which plausibly means that ITCZ might not shift over the equator for strong convection to occur during such extremes. The El Niño event of 2015 is a typical example of such events. We test our results with a more strict criterion by choosing only those events as extremes, which have characteristics similar to that of 1982 and 1997 El Niño events (i.e., Niño3 rainfall > 5 mm day-1 and MSSTG < 0). We declare events having characteristics similar to that of the 2015 event as moderate El Niño events (Fig. S5). Based on this method, we find a robust increase in the number of extreme El Niño events both in 4×CO2 (924 %) and G1 (61 %) at 99 % cl. (Section 3.2.2, page14, lines 26-34)

Minor Points

1)

In P11, L24, the calculation of skewness of SST should be clarified in the context.

Reply:

In the revised manuscript we have made the following changes:

Skewness is a measure of asymmetry around the mean of the distribution (see eq. S1). Positive skewness means that in given data distribution, the tail of the distribution is spread out towards high positive values, and vice versa (Ghandi et al., 2016). (See section 2.4, page 7, lines 2-5)

(See Supplementary, page 13)

S= [1/(n-1)] ($\sum$_$\Theta n(X_i - X\Theta 3)/\sigma$ˆ3 . . . . . (S1; Ghandi

et al., 2016)

Where

S = skewness n = sample size X_i = sample ith observation X ÌĚ = sample mean σˆ3 = sample standard deviation

2)

In P9, L22-24 and P11, L36-39, the independent paragraphs seem abrupt for the context. Better to immerse in the other paragraphs.

Reply:

We have edited and merged the text with other paragraphs as follows:

The weakening of the MSSTG is qualitatively in agreement with previous studies under increased GHG forcings (e.g., Cai et al., 2014; Wang et al., 2017). (see section 3.1.4, page 11, lines 21-22)

Previous studies found that climate models produced mixed responses (both increases and decreases in amplitude) in terms of how ENSO amplitude change with global warming (see Latif et al. 2009; Collins et al. 2010; Vega-Westhoff and Sriver 2017). However, Cai et al. (2018) found an intermodel consensus, for models capable of reproducing ENSO diversity, for strengthening of ENSO amplitude under A2, RCP4.5, and RPC8.5 transient scenarios. (see section 3.2.1, page 13, lines 6-11)

3)

In P12, L6-10, please clarify why quadratic trend to the time series of rainfall data should be excluded.

Reply:

In the revised manuscript, the text has been edited as follows:

To study changes in El Niño frequency, we first need to define what constitutes an El

Niño event. We here define extreme El Niño events as episodes when monthly-mean DJF Niño3 total rainfall exceeds 5 mm day-1, following the threshold definition by Cai et al. (2014). However, as pointed out by Cai et al. (2017), trends in Niño3 rainfall are mainly driven by two factors: (1) the change in the mean state of the tropical Pacific and (2) the change in frequency of extreme El Niño events. Therefore, since we want to focus on the changes in the extremes, we need to remove contribution (1) from the raw Niño3 time series. We, therefore, fit a quadratic polynomial to the time series of rainfall data from which all extreme El Niño events (DJF total rainfall > 5 mm day-1) have been excluded and then subtract this trend from the raw Niño3 rainfall time series. Linearly detrending the rainfall time series produces similar results. (See section 3.2.2, page 14, lines 4-14)

4)

In P13, L13-15, the central Pacific El Nino is not mentioned in the introduction. Also, the question backs to the major comment 1. The HadCM3L may not be able to capture ENSO diversity.

Reply:

We have deleted the referred text from the revised manuscript.

5)

In Figure 4c, why the thermocline depth is not significantly changed over the eastern Pacific. If this is the case, is it due to the choice of 24 isotherms?

Reply:

In a CMIP3 multimodel (SRESA1B scenario) ensemble, Yeh et al. (2009) showed a deepening of the thermocline in the eastern equatorial Pacific; however, Nowack et al. (2017) did not find any change under 4xCO2. Both studies defined thermocline using a maximum vertical temperature gradient. Thus, we believe that no-significant-change in the eastern Pacific is not due to the choice of 24 oC isotherm, but rather due to a

cancellation of competing effects on thermocline depth. In the revised manuscript, we have therefore added the following text:

In 4xCO2, most likely the weakened easterlies (as noticed in Sect. 3.1.3; e.g., Yeh et al., 2009, Wang et al., 2017) and greater ocean temperature stratification due to increased surface warming (see Sect. 4 and Cai et al., 2018) lead to a significant shoaling of the thermocline across the western and central equatorial Pacific. In contrast, relatively little change takes place between 130o W and 90o W. In a CMIP3 multimodel (SRESA1B scenario) ensemble, Yeh et al. (2009) found a more profound deepening of the thermocline in this part of the eastern equatorial Pacific; however, for example, Nowack et al. (2017) did not find such changes under 4xCO2 (cf. their Fig. S9). One possible explanation for this behaviour is the competing effects of upper-ocean warming (which deepens the thermocline) and the weakening of westerly zonal wind stress, causing thermocline shoaling (see Kim et al. 2011a). (see section 3.1.5, from page 11 and line 37 to next page line 8)

6)

The significance level is 90% for differences between G1, 4_CO2 and piControl. How about 95% or even 99%? Will the significant regions be much less?

Reply:

All statistics have been recalculated either with a 95 % or 99 % confidence level. See the manuscript with track changes.

7)

In P23, the height of color bars for figures can be smaller to enlarge the main part of figures. In Figure 2 d & e, symmetric colors are better to represent the negative and positive shadings.

Reply:

In the revised manuscript, all figures have been re-plotted with relatively small and diverging color bars.

8)

In Figure 6 d & e, it's better to set the color bar range with the same ratio as in Figure 5 d & e.

Reply:

In the revised manuscript, both figures are re-plotted with the same color range.

NB. Please see supplementary for figure captions.

Please also note the supplement to this comment:
https://acp.copernicus.org/preprints/acp-2018-1312/acp-2018-1312-AC2-supplement.pdf

---

Interactive comment on Atmos. Chem. Phys. Discuss., https://doi.org/10.5194/acp-2018-1312, 2019.

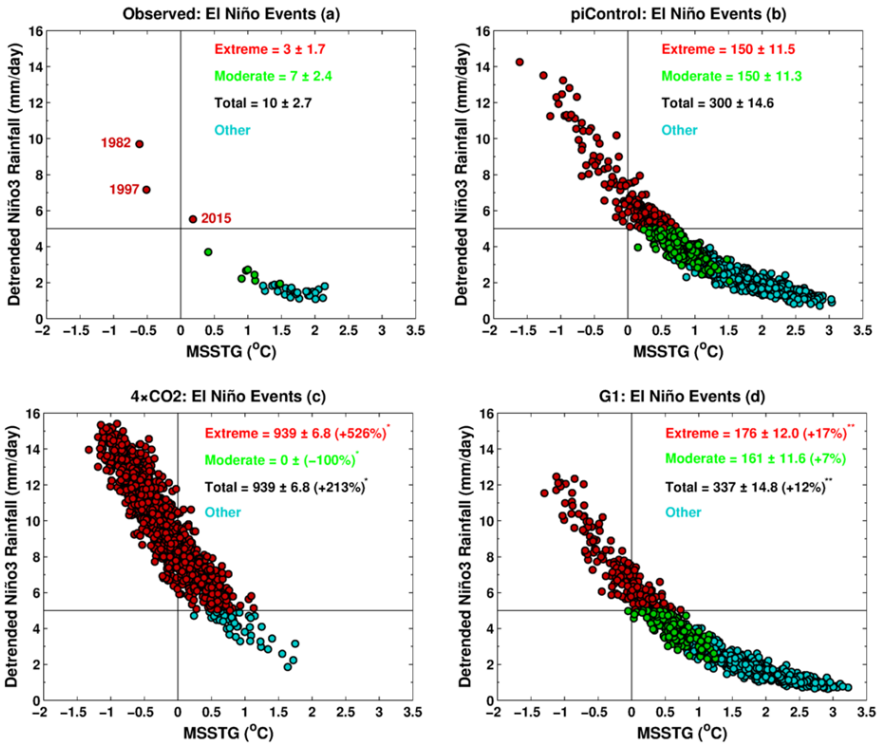

Fig. 1. Figure 7.

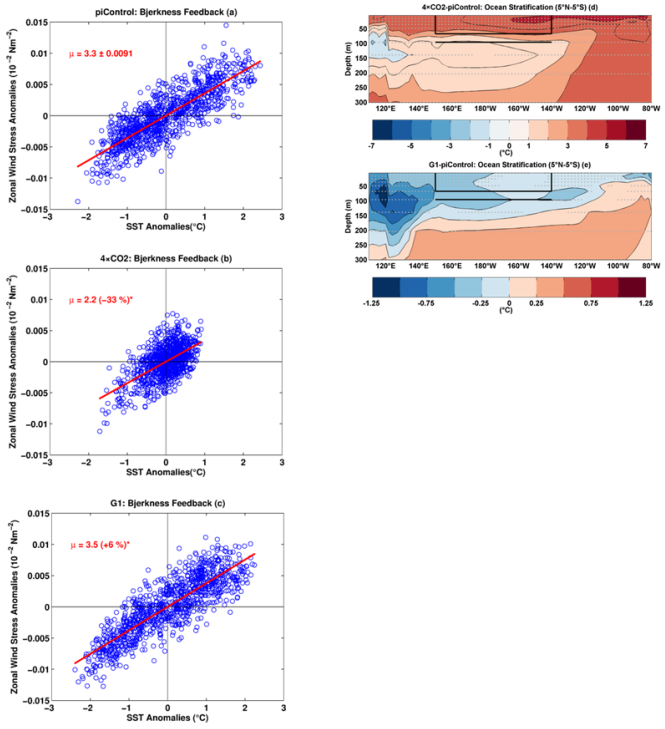

Fig. 2. Figure 15.

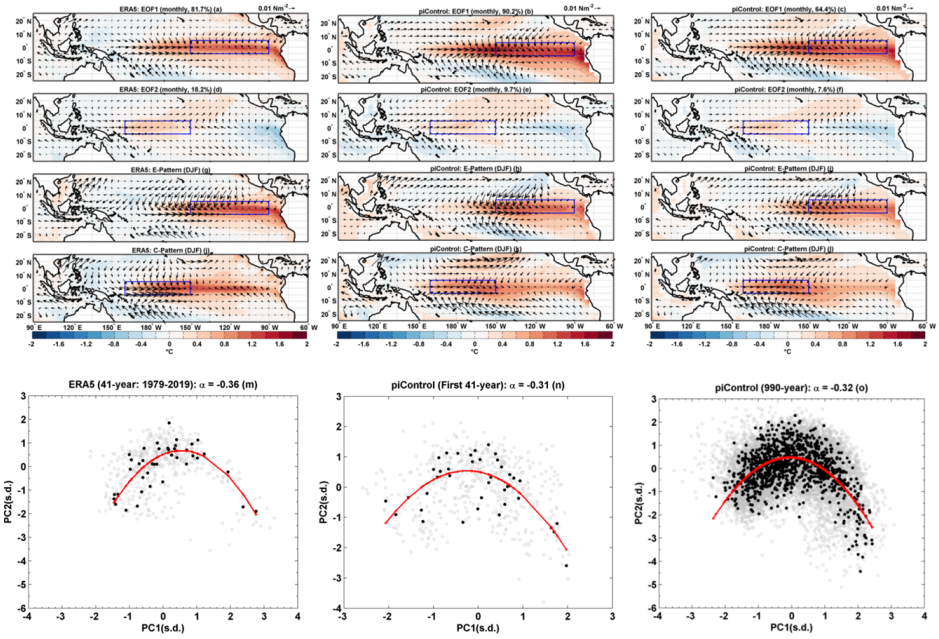

Fig. 3. Figure S1

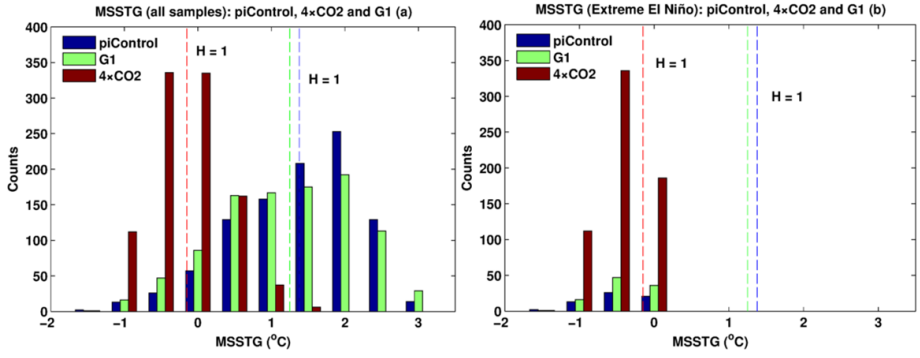

Fig. 4. Figure S3

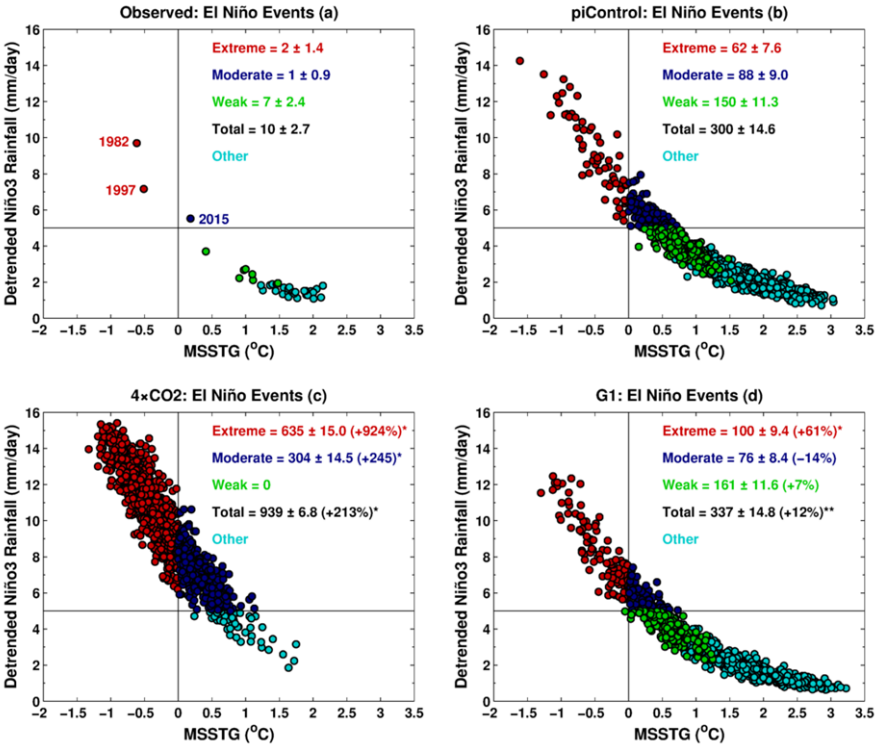

Fig. 5. Figure S5

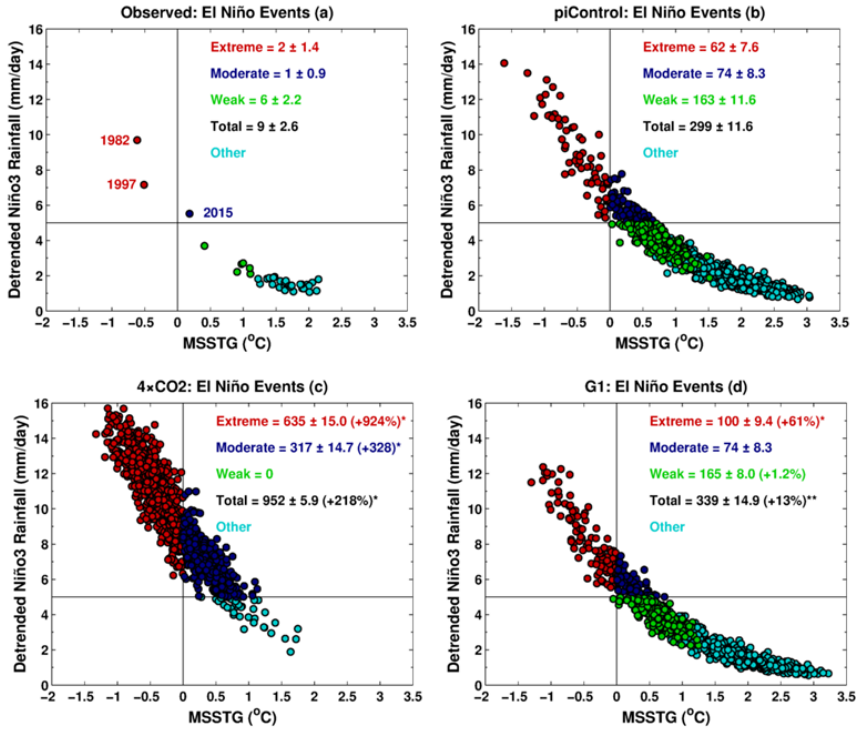

Fig. 6. Figure S6

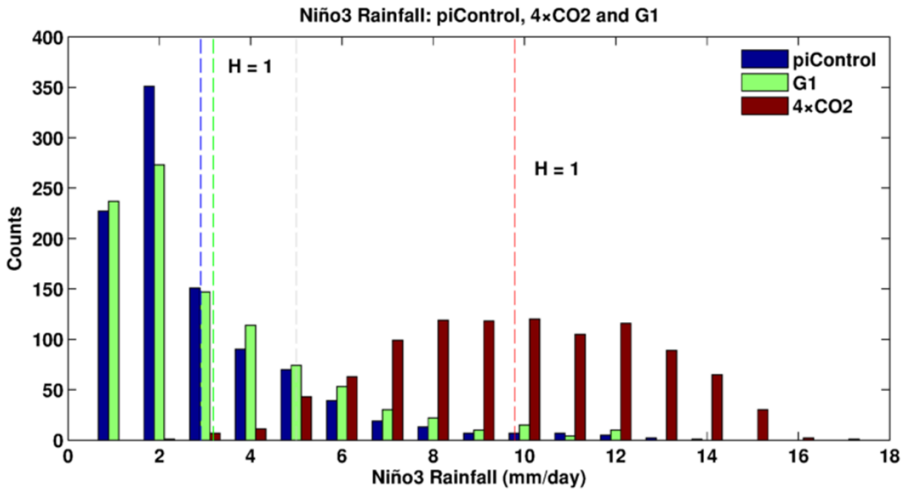

Fig. 7. Figure S8

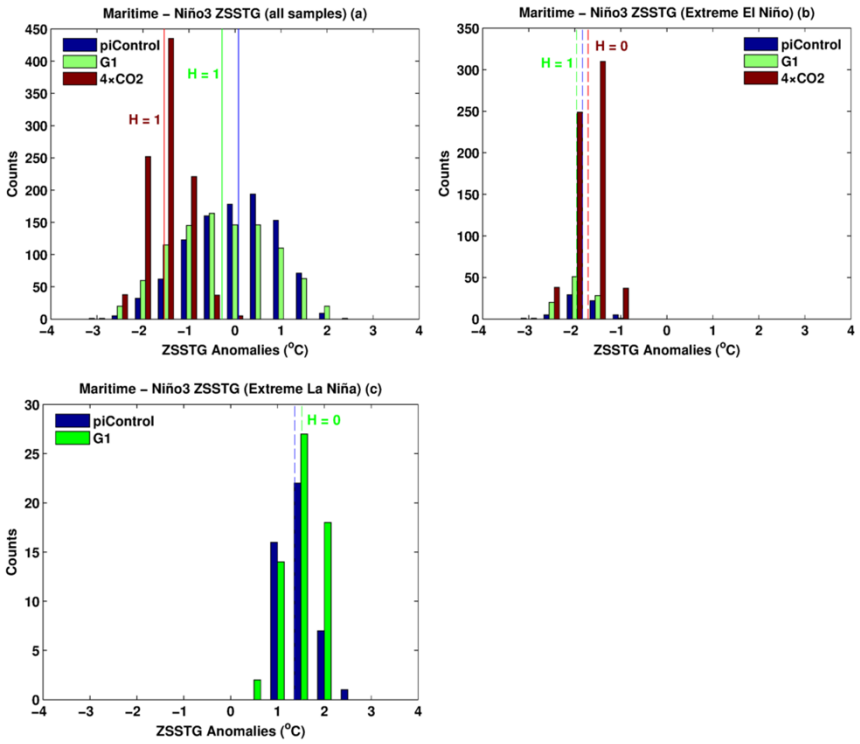

Fig. 8. Figure S9

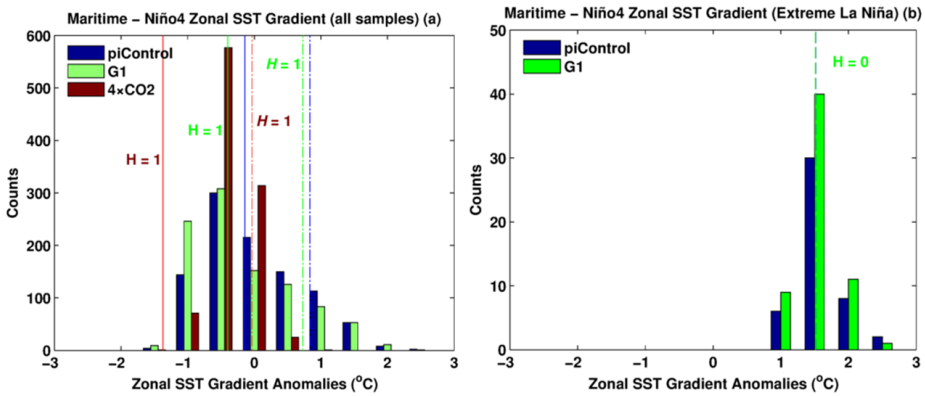

Fig. 9. Figure S10

Table S2. Meridional SST Gradient (MSSTG)

Experiment	Mean (°C)	Difference w.r.t. piControl (°C)	Std. Dev. 10,000 Realizations (°C)	~ Change w.r.t. piControl (%)
piControl	1.38*		0.0265	
4×CO_2	-0.15*	-1.53		-111*
G1	1.25*	-0.13		-9*

Key: *99 % cl; **95 % cl

Fig. 10. Table S2

Table S3. Total number of El Niño events (SST > 0.5 s.d.)

Experiment	No. of Events	Difference w.r.t. piControl	Std. Dev. 10,000 Realizations	~ Change w.r.t. piControl (%)
piControl	300 [300]		14.6 [14.6]	
4×CO_2	161 [565]	139 [265]		-46* [+88*]
G1	337 [337]	37 [37]		+12** [+12**]

Key: Niño3 [E-Index]; *99 % cl; **95 % cl

Fig. 11. Table S3

Table S5. Mean DJF Heat Flux (hf) Feedback

Experiment	hf feedback or Damping Coefficient ($Wm^{-2}/^oC$)	Difference w.r.t. piControl ($Wm^{-2}/^oC$)	Std. Dev. 10,000 Realizations ($Wm^{-2}/^oC$)	~ Change w.r.t. piControl (%)
ERA5	-14.59			
piControl	-14.70		0.52	
4×CO_2	-21.90	+7.19		+48*
G1	-14.85	+0.15		+1.0

*99% cl; **95% cl; Calculation period: ERA5 (41-yrs); HadCM3L (990-yrs)

Fig. 12. Table S5

Table S6. Mean DJF Bjerknes (BJ) Feedback

Experiment	BJ feedback (10^{-2} $Nm^{-2}/^oC$)	Difference w.r.t. piControl (10^{-2} $Nm^{-2}/^oC$)	Std. Dev. 10,000 Realizations ($Wm^{-2}/^oC$)	~ Change w.r.t. piControl (%)
ERA5	3.3			
piControl	3.3		0.0091	
4×CO_2	2.2	-1.1		-33*
G1	3.5	+0.2		+6*

*99% cl; **95% cl; Calculation period: ERA5 (41-yrs); HadCM3L (990-yrs)

Fig. 13. Table S6

Table S7. Mean DJF Ocean Stratification

Experiment	Stratification (^oC)	Difference w.r.t. piControl (^oC)	Std. Dev. 10,000 Realizations (^oC)	~ Change w.r.t. piControl (%)
piControl	2.28*		0.0331	
4×CO_2	5.06*	+2.78		+122*
G1	2.37*	+0.09		+4**

*99% cl; **95% cl

Fig. 14. Table S7